Available online at www.sciencedirect.com

SciVerse ScienceDirect

Acta Materialia 60 (2012) 5322–5334

Acta MATERIALIA

www.elsevier.com/locate/actamat

# Mechanical behavior of carbon fiber composite lattice core sandwich panels fabricated by laser cutting

J. Xiong [a,b], L. Ma [a], A. Vaziri [b], J. Yang [a], L. Wu [a,*]

[a] Center for Composite Materials and Structures, Harbin Institute of Technology, Harbin 150001, China
[b] Department of Mechanical and Industrial Engineering, Northeastern University, Boston, MA 02115, USA

Received 1 April 2012; received in revised form 31 May 2012; accepted 1 June 2012

**Abstract**

This paper presents a novel method for rapid fabrication and prototyping of low-density carbon fiber sandwich panel cores based on laser beam cutting (LBC). Using LCB, sandwich panels with lattice core constructions with oblique and vertical strut morphologies were fabricated from two fiber-orientation architectures. Scanning electron microscopy images illustrate the relatively small extent of damage from laser cutting. The shear strength of the lattice cores was improved by eliminating core-to-face sheet bond failures. Crushing and shear responses of fabricated truss cores were measured, and analytical models are presented to predict the stiffness, strength and dominant failure modes under each loading condition. The sandwich-panel cores investigated appear to be promising candidates for lightweight systems and multifunctional applications.


*Keywords:* Composite; Lattice structure; Laser beam cutting; Mechanical properties

## 1. Introduction

The multifunctional application of cellular structures has been accelerated by the emergence of novel manufacturing techniques that enable fabrication of low-density lattice structures from a variety of engineering materials, including aluminum alloys [1–3], steel wires [4], fiber reinforced polymers [5–8], self-propagating polymer [9], rapid three-dimensional printing materials [10] and hollow-tube microlattices [11]. In this context, fiber reinforced composite cellular structures provide a unique opportunity to develop lightweight multifunctional structural systems, owing to their unique structural and thermal properties. The effort to fabricate composite sandwich panels with low-density lattice core construction has led to the development of several manufacturing techniques, including hot press molding [12–14], pultruded unidirectional fiber-reinforced composite rods without helical forming [15] and water-jet cutting [16]. Two key challenges that limit the application of composite sandwich panels are the slow and costly processes associated with the current manufacturing techniques, and the low quality of the core-to-face sheet bonding [12–16], which is generally the "weakest link" of the panels. Indeed, the design of the core-to-face sheet bond is of great importance, as it dictates the maximum shear load that can be transferred from the face sheets to the core [17–19]. When the node–face sheet interfacial strength is compromised by poor joint design or inadequate bonding methods, premature failure of the sandwich panel occurs. Indeed, bond failure has been identified as a common failure mode for composite sandwich structures [12,13,16,20–22].

Here, a novel and practical method of fabricating composite sandwich panels with lattice cores is introduced, which addresses both challenges discussed above. The method is based on laser-perforating carbon fiber

* Corresponding author. Tel.: +86 451 86412549; fax: +86 451 86402386.
*E-mail addresses:* xiongjian0309@126.com (J. Xiong), wlz@hit.edu.cn (L. Wu).

1359-6454/$36.00 
http://dx.doi.org/10.1016/j.actamat.2012.06.004

corrugated core with large, flat upper and lower bonding surfaces. This method results in composite sandwich panels with lattice cores and high node-to face sheet bond strength. A key advantage of this method is the high rate of cutting and manufacturing, which provides an economic way of manufacturing all-composite sandwich panels. As an example, a pyramidal lattice core with 3 × 3 unit cell can be cut in half an hour, compared with hot press molding and electro-discharge machining methods, which require 4 h and 8 h, respectively, for manufacturing a same-size specimen. The application of laser cutting in fabricating metallic triangular honeycombs was demonstrated by Wei et al. [23]. The present paper extends the application of this technique to composite lattice cores, while also addressing another critical manufacturing issue related to composite panel performance, namely the weak bonding area. Moreover, analytical models are presented to predict the stiffness, strength and dominant failure modes under each loading condition and to provide the insight required for designing high-performance composite sandwich panels.

The details of fabricating the lattice cores with two different strut morphologies, and scanning electron microscopy (SEM) images showing the extent of damage to the composite due to laser beam cutting (LBC), are presented in Section 2. In Section 3, analytical models are developed for the crushing (i.e. out of plane compression) and shear response of pyramidal-like cores with either "oblique" or "vertical" strut morphology. In Sections 4 and 5, the mechanical properties and failure modes are studied experimentally and compared with analytical predictions. Section 6 discusses the specific stiffness and specific strength of fabricated composite lattice cores. A comparison with the shear strength of composite pyramidal truss cores made by other methods is presented in Section 7. Conclusions are drawn in Section 8.

## 2. Fabrication method

The details of the laser cutting method for rapid fabrication and prototyping of composite lattice core structures are presented in this section. Here, the method is applied to create sandwich panels with pyramidal truss-like cores. However, the approach is readily extendable to tetrahedral and multilayer lattices. Fig. 1 illustrates the manufacturing of "oblique" and "vertical" strut morphologies. The precursor carbon fiber composite corrugated cores were laminated in a heated mold from unidirectional carbon fiber/epoxy prepreg sheets with thickness 0.15 mm (T700/epoxy composite; Beijing Institute of Aeronautical Materials, China). The properties of a multilayer flat sheet of 0° fibers cured in optimal conditions are listed in Table 1. The mechanical properties of struts were obtained by testing a composite laminate with a similar stacking sequence. The composite was cured in a hot press at a constant pressure 0.5 MPa and temperature 130 °C for 1.5 h. The composite corrugated cores were detached from the mold after the solidification of the resin.

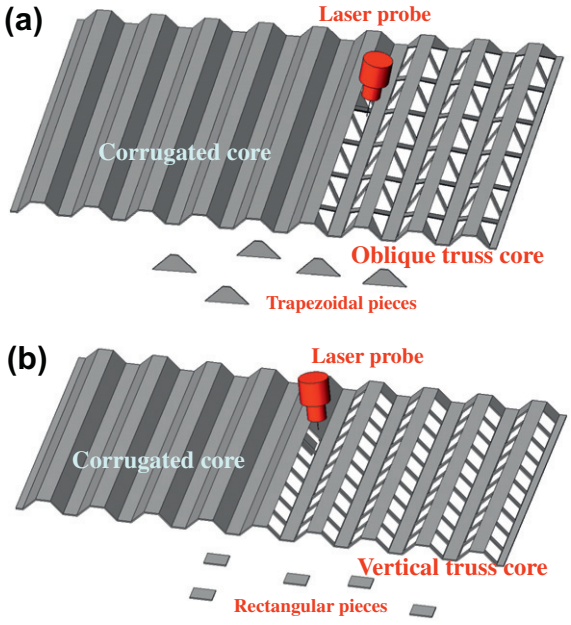


Fig. 1. Schematic of the manufacturing process of the pyramidal truss-like core using the LBC method. The dimensions of removed pieces are also included in the figure. (a) Oblique pyramidal truss-like core. (b) Vertical pyramidal truss-like core.

Table 1
Properties of unidirectional lamella (T700/epoxy composites).

| Properties | Value |
|---|---|
| 0° Tensile strength (MPa) | 1400 |
| 0° Tensile modulus (GPa) | 123 |
| 90° Tensile strength (MPa) | 18 |
| 90° Tensile modulus (GPa) | 8.3 |
| 0° Compression strength (MPa) | 850 |
| 0° Compression modulus (GPa) | 100 |
| 90° Compression strength (MPa) | 96 |
| 90° Compression modulus (GPa) | 8.4 |
| In-plane shear strength (MPa) | 16.0 |
| In-plane shear modulus (GPa) | 4.8 |
| Interlayer shear strength (MPa) | 60 |
| Poisson's ratio | 0.3 |
| Volume fraction of fibers | 57% ± 3 |
| Density (kg/m$^3$) | 1550 |

For "oblique" pyramidal truss-like cores, where strut azimuthal planes are at an angle to the corrugation ridges, corrugated carbon fiber core was manufactured by the hot-press molding method in two styles. Design 1 (half of the fibers aligned with the strut) used a carbon/epoxy layup with [−35°/+35°/−35°/+35°/−35°/+35°]. Owing to the oblique angle of the strut, one family of fibers is always oriented along the strut axis. Design 2 (no fibers aligned) used a layup with [0°/90°/0°/90°/0°/90°]. In this case, no fibers are aligned with the strut axis. For the "vertical" (non-oblique) case, with the strut's azimuthal plane perpendicular to the corrugation ridges, the carbon fiber composite corrugated cores used a layup with [0°/90°/0°/90°/0°/90°], i.e. with half of the fibers aligned with the struts, for direct

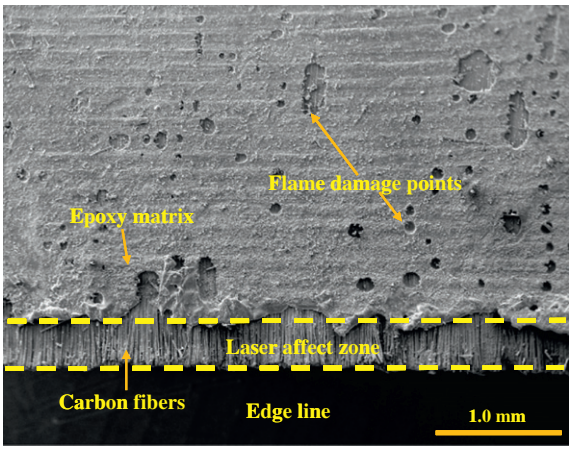


Fig. 2. SEM picture of strut's edge affected by LBC.

comparison with design 1 of the oblique construction. (However, a purely uniaxial layup might be stronger for sandwich panel shearing perpendicular to the corrugation ridges.)

In either case, the corrugated core is then cut vertically by a high-energy laser to form the struts. Fig. 1a and b illustrates the resulting truss-like core and Fig. 3a defines the geometry of the cut holes when projected horizontally on a vertical plane aligned with the corrugation ridges. During cutting, the core is not touched physically by the laser. In principle, this process is capable of holding quite close tolerances, as dictated primarily by the mechanical rigidity of the laser translation stage and specimen support table; however, the depth of the damaged zone makes dimensions relatively imprecise.

The following process parameters were used to cut the carbon fiber composite materials: laser energy 2–3 J pulse$^{-1}$; laser frequency 22–30 Hz; cut speed 1–2 mm s$^{-1}$ and pulse width 1.7–2.5 ms. Fig. 2 shows SEM images acquired from the cut edge of a vertical-style strut. The SEM images of the edge show that ~0.4 mm of the composite adjoining the cut is damaged. In the strongly affected zone, the matrix is almost gone, and carbon fibers are exposed without any epoxy matrix. The carbon fibers are almost intact, as they have a very high melting point and are therefore not affected significantly by laser cutting. Flame damage, caused by laser sparks, was observed approximately through the whole width of struts, with most damage close to the strongly affected zone. It was assumed that the adverse effect of the flame damage on mechanical properties is negligible and, therefore, this effect was neglected in the analytical models.

After being cut, the cores were bonded to both face sheets with epoxy adhesive (08-57; Heilongjiang Petrochemical Institute). The adhesive layer was cured in a hot press at constant pressure of 0.5 MPa and temperature 60 °C for 1.5 h. The process results in a sandwich panel in which the sheet-to-core adhesive area is enlarged to improve the node–face sheet interface strength. The unit cells of each pyramidal truss cores are shown in Figs. 3a and 4a. The relative densities (i.e. volume fraction) of near-pyramidal, cut-from-corrugated truss core in oblique configurations, denoted by $\bar{\rho}$, are given by

$$\bar{\rho} = \frac{2tW[h/\sin\theta - l - t\tan(\theta/2)] + 4tbW + 4tdl/\cos\alpha}{WL(h+t)} \quad (1)$$

where $b$, $d$, $h$, $t$ and $\theta$ are geometrical parameters shown in Figs. 3a and 4a. The vertical struts morphology is a special case of oblique struts morphology, where $\alpha = 0°$. $l$ and $a$ are shown in Fig. 3(a). (Note that d is measured perpendicular to a strut, not horizontally.) $L = 4b + 2h/\tan\theta - 2t\tan(\theta/2)$ is the corrugation wavelength from trough to trough, and $W = 2a + 2d/\cos\alpha + 2l\tan\alpha$ are the widths along the corrugation ridge direction of oblique and vertical pyramidal truss-like cells.

Figs. 3b and 4b show photographs of the oblique and vertical pyramidal truss-like core sandwich structures. The illustrated sample of oblique has dimensions $t = 0.9$ mm, $a = 8$ mm, $b = 4.75$ mm, $d = 4$ mm, $h = 12$ mm, $l = 14$ mm, $\theta = 45°$ and $\alpha = 35°$, resulting in predicted relative densities of 4.99% (Fig. 3b), and the vertical pyramidal

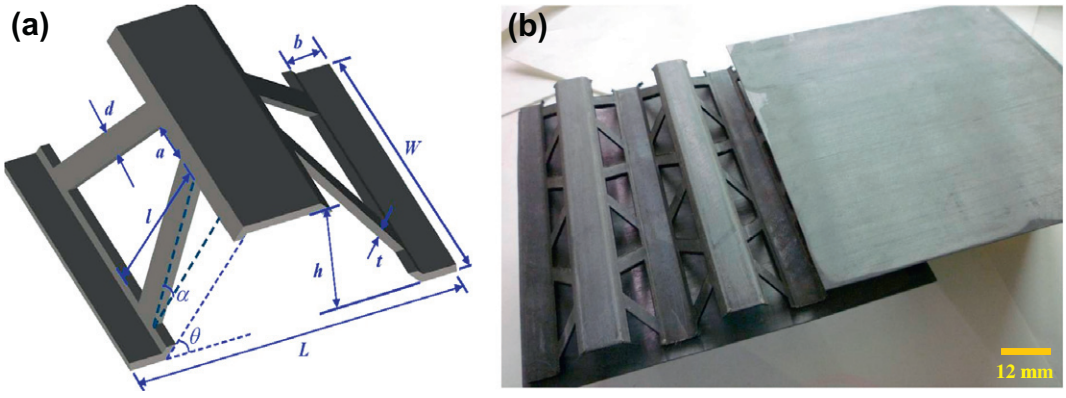


Fig. 3. (a) Sketch of the unit cell of the oblique pyramidal truss-like core. (b) Photograph of a carbon fiber composite oblique pyramidal truss-like core sandwich structure (design 1). The core relative density is 4.99%.

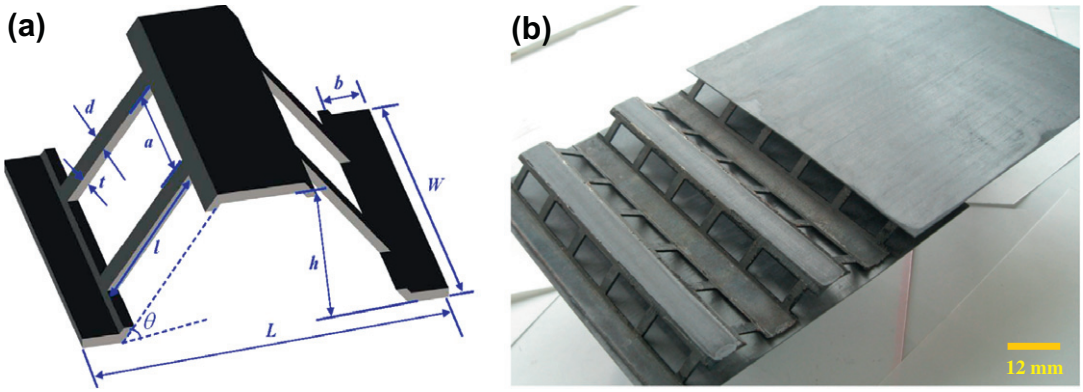


Fig. 4. (a) Sketch of the unit cell of the vertical pyramidal truss-like cores. (b) Photograph of a carbon fiber composite vertical pyramidal truss-like core sandwich structure. The core relative density is 4.77%.

truss-like core sandwich structures with relative core density 4.77% shown in Fig. 4b has $a = 20$ mm, $\alpha = 0°$, and each strut of the pyramidal truss is made of six slender laps.

## 3. Analytical models for core crushing and shear responses

Sandwich structures are typically subjected to significant shear and bending loads. The flexural stiffness and strength of the panel are determined by the core shear properties [25]. In addition, core compressive strength may be important in supporting concentrated loads [26–28]. In this section, analytical models for the crushing and shear response of pyramidal truss-like cores are developed by analyzing the elastic deformation of a single strut of a pyramidal truss-like core. The stiffness models are based on both axial and flexural stiffness of the core struts [29,30]. The strength models are based on the axial loads applied to each strut when the panel is subjected to a shear or compressive load. Euler buckling and compressive fracture of the composite struts are the two competing failure modes. The framework for analysis of individual struts of a pyramidal-like core with oblique strut morphology is shown in Fig. 5a: the vertical strut morphology is a special case with $\alpha = 0°$.

Because of unit-cell symmetry, loads along any coordinate axis will result in displacement along that axis. Therefore, calculations can be made by considering displacements along the coordinate directions, in which case each strut contributes exactly 1/4 of the total stiffness.

For $A(x_o, y_o, z_o)$, $x_o = y_o = z_o = 0$. (See Fig. 5b.)

For $B(x_1, y_1, z_1)$, $x_1 = l\cos\theta$, $y_1 = l\sin\theta\sqrt{\csc^2\theta\sec^2\alpha - 1 - ctg^2\theta}$, $z_1 = l\sin\theta$.

The length of the single strut $l_{AB}$ and the deformation of the single strut $\Delta l_{AB}$ are found as follows:

$$l_{AB} = \sqrt{(x_1 - x_0)^2 + (y_1 - y_0)^2 + (z_1 - z_0)^2} = l\sec\alpha \tag{2}$$

$$\Delta l_{AB} = \left[\delta_x \quad \delta_y \quad \delta_z\right]\left[\frac{x_1 - x_0}{l_{AB}} \quad \frac{y_1 - y_0}{l_{AB}} \quad \frac{z_1 - z_0}{l_{AB}}\right]^{-1} = \delta_x\frac{x_1 - x_0}{l_{AB}} + \delta_y\frac{y_1 - y_0}{l_{AB}} + \delta_z\frac{z_1 - z_0}{l_{AB}} \tag{3}$$

### 3.1. Compressive stiffness and strength

For an imposed displacement $\delta_z$ in the $z$ direction, $\delta_x = 0$, $\delta_y = 0\delta_z \neq 0$. The analytical calculations are similar to previous work [13], and the details are provided in the Appendix A for the sake of brevity. The results are summarized below.

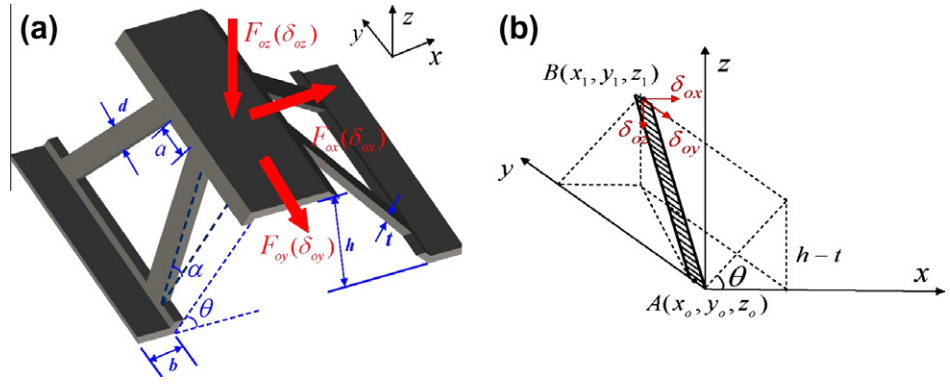


Fig. 5. (a) Unit cell of a oblique pyramidal truss-like core subjected to compressive and shear loading. (b) Schematic of a single strut deformation of oblique pyramidal truss-like core.

The effective Young's modulus of the pyramidal truss structure is

$$E_z = 4E_s \sin\theta\cos^2\alpha\frac{dt}{WL} \times \frac{h+t}{l}\left[\sin\theta\cos\alpha + \frac{t^2\cos\alpha(1-\sin^2\theta\cos^2\alpha)}{l^2\sin\theta}\right] \quad (4)$$

Two failure mechanisms for the core struts under crushing are elastic buckling and fracture. The analytical models for predicting the failure stress associated with each failure mechanism are provided in Appendix A, and yield

$$\sigma_{zE} = \frac{\pi^2}{3}\frac{t^2}{l\sin\theta(h+t)}E_z \quad (5)$$

$$\sigma_{zC} = \frac{E_z}{E_s}\frac{l}{h+t}\frac{1}{\sin\theta\cos^2\alpha}\sigma_C \quad (6)$$

where $\sigma_{zE}$ and $\sigma_{zC}$ are the nominal strength of the core associated elastic buckling and fracture of struts under crushing, respectively.

### 3.2. Shear stiffness and strength

#### 3.2.1. Shearing in x direction

In this case, $\delta_x \neq 0$, $\delta_y = 0$, $\delta_z = 0$. The effective shear stiffness of the lattice core, denoted by $G_x$, can be estimated from (see Appendix A for details)

$$G_x = 4E_s\cos\theta\cos^3\alpha\frac{dt}{WL} \times \frac{h+t}{l}\left[\cos\theta + \frac{t^2(1-\cos^2\alpha\cos^2\theta)}{l^2\cos\theta} + \frac{d^2}{l^2\cos\theta}\right] \quad (7)$$

To estimate the collapse strength of the pyramidal core under shear along the $x$ direction, two different failure mechanisms were considered, similar to those in Section 3.1. The Euler buckling load of an end-clamped strut subjected to an axial load can be estimated from $F_A = F_{xE} = \pi^2E_sdt^3\cos^2\alpha/3l^2$, where $E_s$ is the strut's compressive stiffness. The nominal shear strength of a pyramidal truss core can be estimated from

$$\tau_{xE} = \frac{\pi^2}{3\cos\theta}\frac{t^2}{l(h+t)}G_x \quad (8)$$

The fracture load of a composite strut is $F_A = F_{xC} = \sigma_C dt$, where $\sigma_C$ is the strut's fracture strength. The shear stress associated with the onset of strut fracture, $\tau_{xC}$ can be estimated from

$$\tau_{xC} = \frac{G_x}{E_s}\frac{1}{\cos\theta\cos^2\alpha}\frac{l}{h+t}\sigma_c \quad (9)$$

#### 3.2.2. Shearing in y direction

In this case, $\delta_x = 0$, $\delta_y \neq 0$, $\delta_z = 0$. Following the same approach as in the previous sections gives an estimate of the shear stiffness

$$G_y = \frac{4E_s\sqrt{1-\sin^2\theta\cos^2\alpha}\cos^2\theta\cos^2\alpha}{\sin\alpha}\frac{dt}{WL} \times \frac{h+t}{l}\left[\cos\theta + \frac{t^2(1-\cos^2\theta\cos^2\alpha)}{l^2\cos\theta} + \frac{d^2}{l^2\cos\theta}\right] \quad (10)$$

The collapse strength under shear along the $y$ direction associated with Euler buckling and crushing of struts can be calculated in a similar way to the previous section. These yields

$$\tau_{yE} = \frac{\pi^2}{3\cos\theta}\frac{t^2}{l(h+t)}G_y \quad (11)$$

$$\tau_{yC} = \frac{G_y}{E_s}\frac{1}{\cos\theta\cos^2\alpha}\frac{l}{h+t}\sigma_c \quad (12)$$

The estimated shear strengths in the $x$ and $y$ directions are different from each other, in contrast to the behavior of other pyramidal truss cores [31,32]. For the oblique struts, since $\tau_{yE} < \tau_{xE}$ and $\tau_{yC} < \tau_{xC}$, shear stiffness and strength were measured in the $x$ direction only. Also for the vertical pyramidal truss-like cores, $\tau_{yE} = \tau_{yC} \approx 0$. Since $\tau_{yE} \ll \tau_{xE}$ and $\tau_{yC} \ll \tau_{xC}$, in the following experimental section, shear stiffness and strength were measured in the $x$ direction only. Failure maps of lattice cores are plotted in Section 6, to provide a quantitative comparison between different failure mechanisms of lattice cores and the relationship between the dominant failure mechanisms and lattice core design and geometrical configuration.

## 4. Experimental protocol

Uniaxial compression and shear tests were carried out using a screw-driven testing machine (INSTRON 5569) following ASTM C365 and C273 [33,34]. The applied load was measured via the load cell of the test machine, while a laser extensometer was used to measure the nominal axial strain in the specimens. The shear test set-up with pyramidal truss-like cores is shown in Fig. 8. The specimen size was at least $3 \times 6$ unit cells. All the tests were carried out quasi-statically with a nominal displacement rate of $0.5\,\text{mm}\,\text{min}^{-1}$, and at room temperature. Unloading–reloading curves were used to determine the apparent elastic properties and collapse strength.

## 5. Summary of the measured responses

Feih et al. [24] suggested that, when a composite laminate is heated beyond a critical softening temperature, both stiffness and strength decrease with increasing temperature to a minimum value that is generally negligible. The increase in temperature induced by laser cutting is much higher than the critical softening temperature of the composite laminates. Thus, it is assumed that the remaining strength and stiffness of the composite in the strongly affected zone is negligible. The original width of the strut $d$ is 4 mm, and the strongly affected zone is measured as

0.4 mm so, accounting for both sides of the cut, the effective width "$d_e$" is ~3.2 mm. The effective width was used in the analytical models of lattice structure mechanical properties. However, the original width was used in calculating the lattice core relative density.

### 5.1. Compressive responses

Under compressive loading (crushing), the core-to-sheet adhesive bond is in compression (except perhaps in bonds close to the panel edges), and therefore is not expected to fail. Indeed, no bond failure was observed.

#### 5.1.1. Oblique-strut pyramidal truss-like cores (design 1)

The compressive stress–strain response of sandwich panels with oblique-style cores, with half the strut fibers aligned with the strut axis (design 1), are shown on the left of Fig. 6a, and the corresponding failure modes are shown in the left photograph of Fig. 6b, including Euler buckling, delamination and fracture. Three different core relative densities were investigated. The peak stress for $\bar{\rho} = 3.41\%$ occurs at 0.32 MPa before any visible failure, followed by Euler buckling and the subsequent large bending deformation of struts, as shown in the first pictures. The analytical compressive stiffness and collapse strength of oblique struts can be estimated from Eqs. (4) and (5) as 33.38 MPa and 0.32 MPa. For cores with relative density 4.99% and 7.91%, fracture and delamination of struts are the dominant failure modes shown in the second and third pictures on the left of Fig. 6b. The theoretical stiffness and applied stress associated with the onset of strut fracture can be calculated from Eqs. (4) and (6), as shown in Table 2. For some specimens, the experimental strength results are somewhat higher than the theoretical values. This is probably related to neglecting the residual strength of the laminated composite in the strongly affected zone, as discussed above.

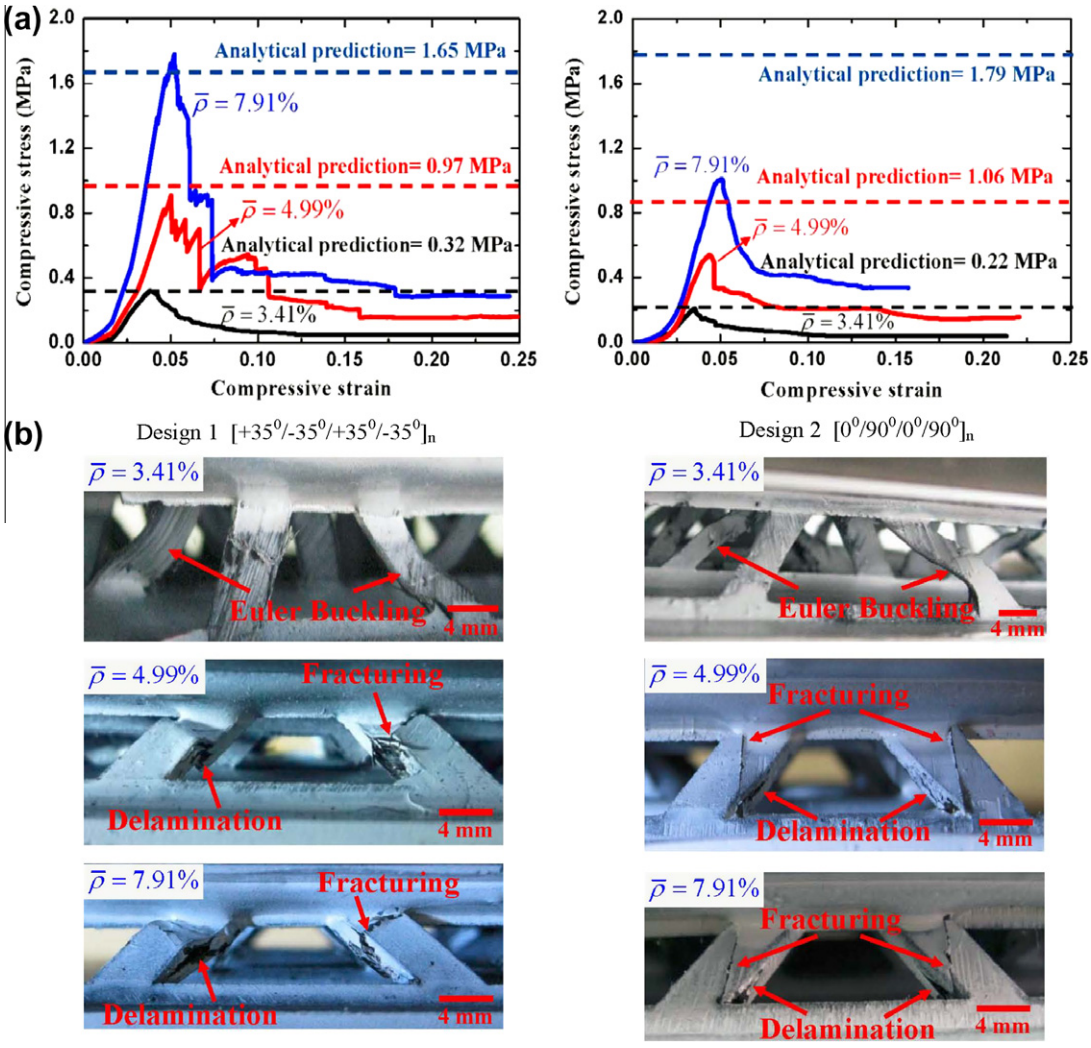


Fig. 6. Compressive behavior of carbon fiber composite pyramidal truss-like cores: Design 1 has half the fibers along each strut, while design 2 has vertical/horizontal fibers in the strut plane: (a) stress vs. strain curve; (b) compressive failure mechanisms (Euler buckling, delaminating and fracturing).

Table 2
Dimensions of the specimens and the predicted and measured failure loads and collapse modes. The failure modes under compression and shear in this table are abbreviated: E = Euler buckling mode; C = crushing mode (delamination and fracturing).

| Specimen | $\rho$ (kg/m$^3$) | $a$ (mm) | $t$ (mm) | $\alpha$ (°) | Analytical | | Experiment | |
|---|---|---|---|---|---|---|---|---|
| | | | | | Fail. mode | fail. stiffness/strength (MPa) | Fail. mode | fail. stiffness/strength (MPa) |
| *Out of plane compression* | | | | | | | | |
| Oblique truss (Design 1) | 52.86 | 8 | 0.6 | 35 | E | 33.38/0.32 | E | 26.34 ± 2.03/0.32 ± 0.03 |
| | | | | | | C 33.38/0.32 | | |
| | 77.35 | 8 | 0.9 | 35 | E | 51.71/1.08 | C | 32.68 ± 2.99/0.91 ± 0.04 |
| | | | | | C | 51.71/0.97 | | |
| | 122.61 | 8 | 1.5 | 35 | E | 92.16/6.38 | C | 63.68 ± 3.18/1.78 ± 0.09 |
| | | | | | C | 92.16/1.65 | | |
| Oblique truss (Design 2) | 52.86 | 8 | 0.6 | 35 | E | 23.94/0.23 | E | 16.94 ± 1.21/0.21 ± 0.04 |
| | | | | | C | 23.94/0.65 | | |
| | 77.35 | 8 | 0.9 | 35 | E | 37.09/0.78 | C | 23.89 ± 2.31/0.54 ± 0.08 |
| | | | | | C | 37.09/1.06 | | |
| | 122.61 | 8 | 1.5 | 35 | E | 66.10/3.66 | C | 40.29 ± 3.87/1.01 ± 0.05 |
| | | | | | C | 66.10/1.79 | | |
| Vertical truss | 50.53 | 20 | 0.6 | 0 | E | 58.21/0.55 | E | 46.76 ± 3.13/0.50 ± 0.03 |
| | | | | | C | 58.21/0.74 | | |
| | 73.94 | 20 | 0.9 | 0 | E | 90.13/1.88 | C | 67.88 ± 2.36/1.03 ± 0.04 |
| | | | | | C | 90.13/1.13 | | |
| | 117.03 | 20 | 1.5 | 0 | E | 160.23/8.87 | C | 117.23 ± 9.59/1.92 ± 0.09 |
| | | | | | C | 160.23/1.91 | | |
| *Shear* | | | | | | | | |
| Oblique truss (Design 1) | 77.35 | 8 | 0.9 | 35 | E | 60.11/1.26 | C | 34.90 ± 3.44/0.91 ± 0.06 |
| | | | | | C | 60.11/1.13 | | |
| | 122.61 | 8 | 1.5 | 35 | E | 106.98/5.93 | C | 60.24 ± 4.54/1.83 ± 0.08 |
| | | | | | | C 106.98/1.91 | | |
| Vertical truss | 73.94 | 20 | 0.9 | 0 | E | 104.67/2.18 | C | 70.15 ± 5.73/0.95 ± 0.09 |
| | | | | | C | 104.67/1.30 | | |
| | 117.03 | 20 | 1.5 | 0 | E | 185.57/10.28 | C | 105.47 ± 7.93/1.52 ± 0.12 |

For Design 1, $E_s = 34.3$ GPa and $\sigma_s = 278.8$ MPa were obtained from the compressive test of a relatively similar laminate with $[0°/90°/0°/90°/0°/90°]_4$. For design 2, $E_s = 24.6$ GPa and $\sigma_s = 303.5$ MPa were also measured from laminate with $[45°/-45°/45°/-45°/45°/-45°]_4$. Here, $E_s$ and $\sigma_s$ are the unloading Young's modulus and the crushing failure strength of the face sheet.

### 5.1.2. Oblique-strut pyramidal truss-like cores (design 2)

The stress–strain behavior of the three relative densities of composite oblique struts with no axial strut fibers (design 2) is shown on the right-hand side of Fig. 6a. The structures showed linear elastic behavior initially, reaching a peak stress at relatively small strain. The peak was followed by a sharp stress drop associated with fiber-direction fracturing (see the right-hand side of Fig. 6b) and progressive crushing. As with design 1, Euler buckling, delamination and fracture of the struts were observed for three different relative densities. From Table 2, the peak measured strengths are considerably below the analytical predictions. This is because none of the fibers aligns with the struts, and the resulting short, angled fibers cannot transmit much axial load. It is clear that design 1 is much better than design 2, because half the fibers are axially aligned with struts. The compressive failures clearly depend strongly on the fiber orientation within the struts.

### 5.1.3. Vertical-strut pyramidal truss-like cores

Vertical pyramidal truss-like cores were designed with an expectation that the out-of-plane compressive strength would be enhanced, due to a reduced buckling length, and a reduced angle between each vertical strut and flat bottom face sheet, and this turned out to be correct. The compressive stress–strain responses of the vertical pyramidal truss-like sandwich panels with three different relative densities are shown in Fig. 7a. The structures exhibited characteristics similar to those of oblique-geometry design 1, including an initial elastic response followed by a peak strength associated with truss Euler buckling, delamination and fracture (Fig. 7b). The peak stress for the vertical pyramidal truss-like core occurred at 0.50 MPa with no visible failure, followed by Euler buckling. The calculated compressive stiffness and collapse strength of the vertical pyramidal-truss core due to the elastic buckling or fracture of its constituent struts can be estimated from Eqs. (4)–(6) with $a = 20$ mm and $\alpha = 0°$. For specimens with relative densities 4.77% and 7.55%, the struts failed by fracturing and delaminating in the middle.

From Table 2, it can be seen that vertical geometry is theoretically much better than oblique geometry under out-of-plane compression. Experimentally, the improvement is not so great but is still significant.

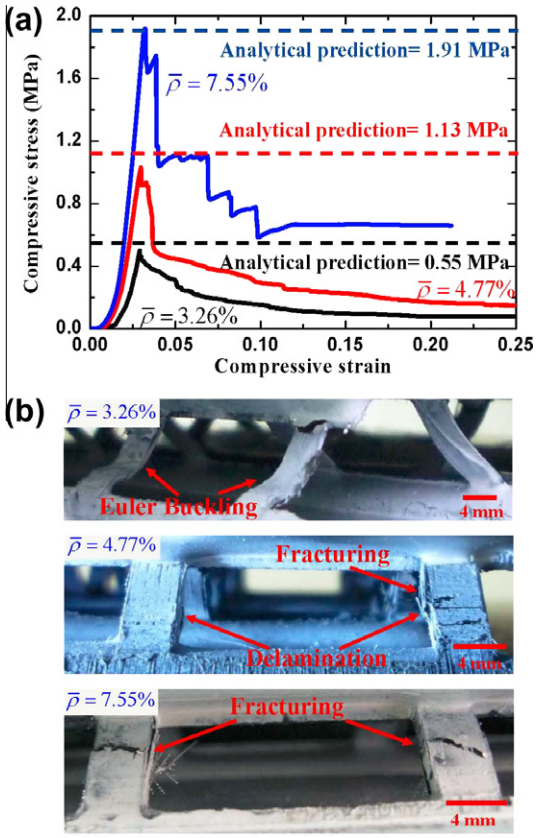


Fig. 7. Compressive behavior of vertical pyramidal truss-like cores sandwich structures: (a) stress vs. strain curve; (b) compressive failure mechanisms.

### 5.2. Shear response

Fig. 9 shows the measured and predicted shear response in the $x$ direction, as well as photographs of the oblique (design 1) and vertical struts. The red dashed arrows mark the shear direction. For the oblique (design 1) struts, an initial linear response was followed by a non-linear regime. Subsequently, the stresses decreased with increasing strain, with the serrations in the load curve being caused by a series of failure events. For the core with vertical struts, the initial linear response is similar to the response of the oblique struts core. However, there was no sudden decrease in the stress and, instead, a relatively wide plateau-like response. In this experiment, it was observed that the fibers were peeled from the face of struts and the back of the adhesive area. This observed failure mode was denoted as "peeling failure". The comparison of analytical predictions and measured values are shown in Table 2.

#### 5.2.1. Oblique-strut pyramidal truss-like cores (design 1)

For the specimens with relative density 4.99% and 7.91%, the peak stresses were 0.91 MPa and 1.83 MPa, and strut delamination was the dominant failure mode, with failure initiating along the strut plies near the ends of struts. The measured failure stress and stiffness (Table 2) for both specimens were lower than the predicted values. It is speculated that the stiffness deviation could be due to imperfect contact with the loading platens, and the strength deviation could be due to mold pressure and temperature inconsistencies in fabricating the composite corrugated cores. Also, the damage due to laser cutting of the struts was not precisely modeled and considered in the analytical models.

#### 5.2.2. Vertical-strut pyramidal truss-like cores

The $x$ direction shear strength was expected to be larger than the strength with oblique struts. For the specimens with core relative densities 4.77% and 7.55%, the peak stresses were 0.95 MPa and 1.52 MPa and, after each peak stress, a plateau was observed. Delamination near the strut end is the dominant failure mode. Some fibers were pushed out from the behind the adhesive area, this is because these peeling fibers are in continuum with the fibers aligned with the struts, and the struts transmit the load from the lower end to behind the adhesive area directly under shear loading. Table 2 shows that the predicted failure stiffness and stress (obtained using Eqs. (7)–(9) with $a = 20$ mm, $\alpha = 0°$) are almost twice as high as the measured values, owing to imperfections in the manufactured specimens and perhaps the unusual failure mode. The shear properties of vertical-strut cores turn out to be worse than oblique-strut properties. The main reason is that the peeling failure of surface layers of struts reduced the overall mechanical properties.

## 6. Specific stiffness and specific strength of lattice truss cores

In Fig. 10, the specific stiffness and specific strength of fabricated core constructions are plotted under both core

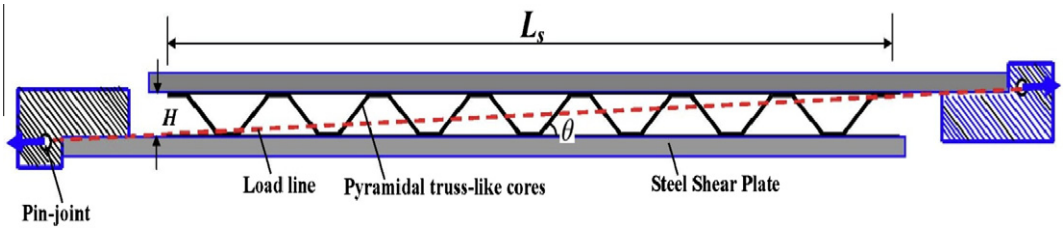


Fig. 8. Schematic of the shear test set-up with pyramidal truss-like cores.

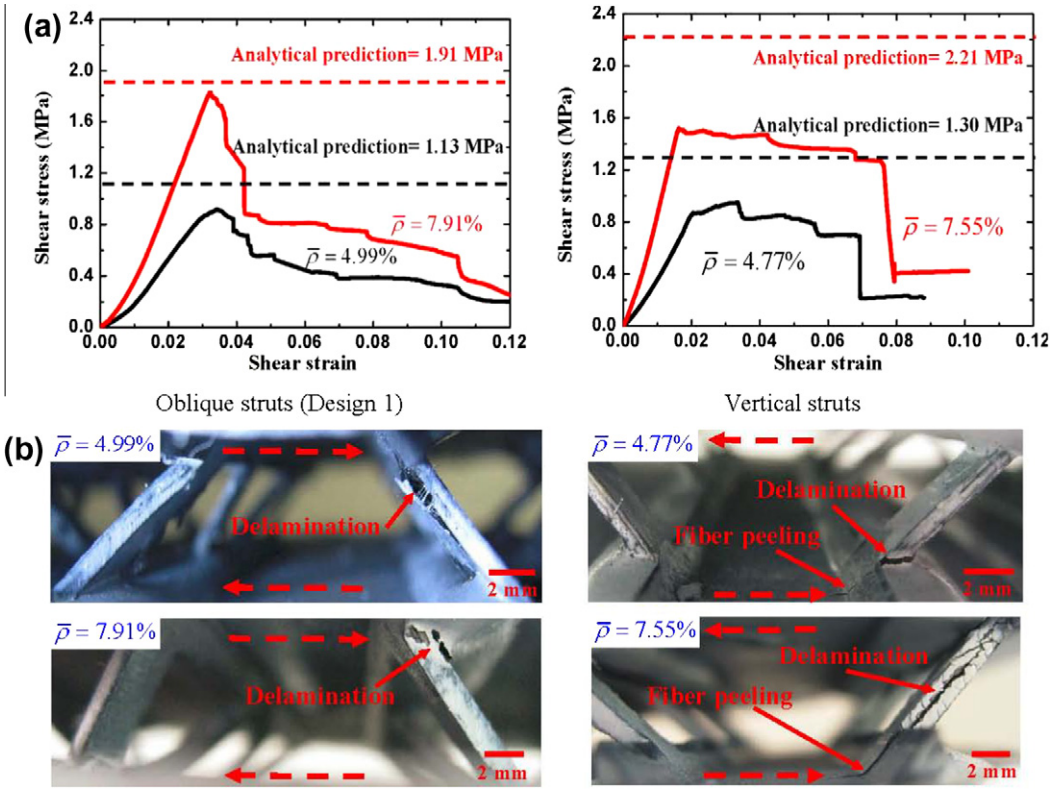


Fig. 9. (a) Shear stress vs. strain curve of oblique and vertical pyramidal truss-like cores. (b) Shear failure mechanisms of both pyramidal truss-like cores (peeling and delaminating). The red dashed-line arrows mark the shear direction. (For interpretation of the references to color in this figure legend, the reader is referred to the web version of this article.)

compression and core shear loadings. The results are plotted as a function of lattice truss core angle $\alpha$, as defined in the insets of Fig. 3. The theoretical values of specific stiffness and specific strength are plotted based on the analytical predictions provided in Section 3 and by considering 20% reduction in the width due to the laser-induced damaged to the struts. The analytical solutions for different strut thickness, $t$ and strut spacing $a$ are plotted as solid lines. The specific compressive stiffness and specific strength under both compression and shear loadings decrease with increasing angle $\alpha$ of lattice truss cores. Increasing the truss angle from 0° to 90° results in lower values of density, stiffness and strength, resulting in overall lower specific stiffness and strength (i.e. increasing the truss angle has considerably more effect on the stiffness and strength values compared with its effect on the reduction in core relative density). It should be noted that the strength of the core is dominated by fracture of the struts, not Euler buckling. The experimental values for lattice structures with $\alpha = 0°$ and 35° from Section 5 are also shown on the same graphs for comparison. In general, the analytical predictions and experimental results are in good agreement. Some experimental values are larger than the analytical predictions, and because the residual strength and stiffness of the strongly affected zone are assumed to be negligible.

Fig. 11 shows the specific compressive and shear strength vs. the strut thickness $t$ for lattice cores with two different geometrical configurations. As expected, buckling is the dominant mechanism for thin struts, while cores with thick struts fail as a result of strut fracture or delamination. For composite lattice core with $\alpha = 0°$ and $\alpha = 35°$, this critical strut thickness is 0.7 mm and 0.85 mm, respectively, as shown in Fig. 11. Here, the specific shear strength is a little higher than the specific compressive strength for both truss lattices considered in Fig. 11. The experimental results are shown using average values and error bars. The critical thickness that denotes the transition between two mechanisms is the same for both compression and shear loading. In general, the specific strength of vertical struts is higher than the strength of lattice cores with oblique struts. The exception is the experimental results denoted by the blue area as "peeling failure", where the strength of vertical struts is compromised by the peeling failure induced in individual struts.

The specific stiffness and specific strength of lattice structures with $\alpha = 35°$ are plotted in Fig. 12, based on the analytical expressions presented in Section 3. If the angles are smaller than the critical angle, the specific shear stiffness and strength are larger than the specific compressive stiffness and strength values. For the specific stiffness and specific strength, this critical angle is 47.2° and 50.2°,

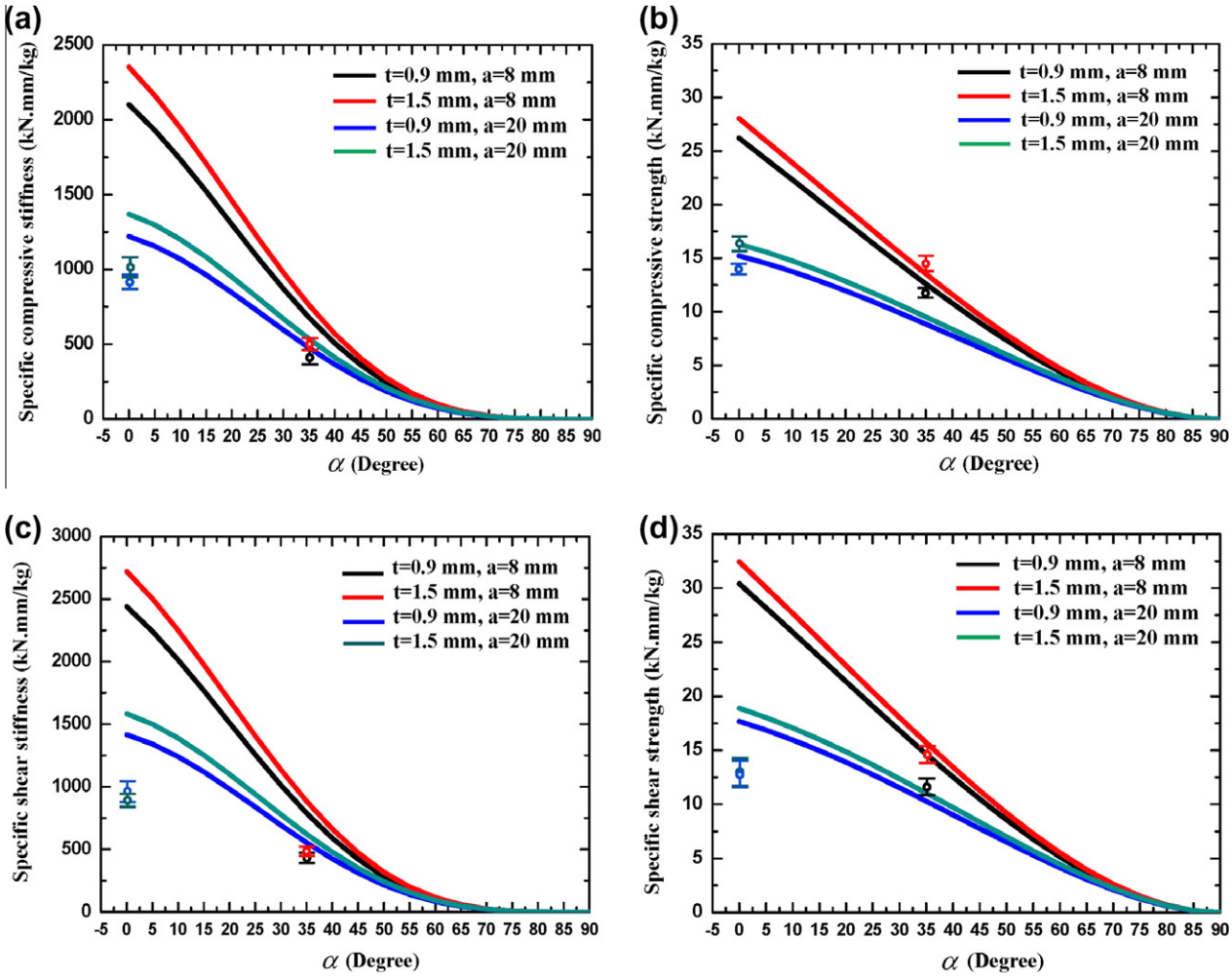


Fig. 10. The plots of (a) specific compressive stiffness, (b) compressive specific strength, (c) specific shear stiffness and (d) specific shear strength as functions of lattice truss core angle. The analytical predictions are plotted as solid lines for lattice structures with different $a$ and $t$. Experimental data are also shown. The data bars denote the maximum and minimum values for different lattice cores. The color of the data bar matches the color of the solid line plotted based on the analytical prediction (example: the red data bar and the red solid line are both associated with the lattice structure with $t = 1.8$ mm and $a = 8$ mm). Here, the following parameters are constant: $b = 4.75$ mm, $d_e = 3.2$ mm, $h = 12$ mm, $l = 14$ mm, $\theta = 45°$. (For interpretation of the references to color in this figure legend, the reader is referred to the web version of this article.)

respectively. It should be noted that this critical strut angle is different for the specific stiffness and specific strength plots. However, the critical angle of lattice truss cores with different strut thickness $t$ is the same for specific stiffness or specific strength. In the current work, all the specimens have a strut angle smaller than the critical angle, and thus the shear stiffness and strength of the fabricated lattice structures are larger than the compressive stiffness and strength values.

## 7. Comparison with other lattice truss cores

Carbon fiber composite pyramidal truss cores made by the hot press method and by the snap-assembly method suffer from core-to-sheet bond failure under out-of-plane compressive and shear loading. These failures initiate at defects or in the small face-sheet to truss-core bonding area under shear loading. The fabrication method described above yields carbon fiber composite sandwich panels in which the truss core–face sheet adhesion area has been increased. Modifying the pyramidal truss configuration to increase the adhesion area results in an increase in the overall weight of the lattice core at the same relative density. Fig. 13 shows the modified Ashby's chart for both compressive strength and shear strength vs. density. The chart is only plotted for materials with low-density materials with density $<2000\ \mathrm{kg\ m^{-3}}$ or so. The results from the current work are shown by a blue area marked "Composite pyramidal truss-like core". The compressive strength of the fabricated structure is located in the middle of the chart. As expected, there is no gain from increasing the adhesive area in the compressive strength of the lattice cores. In the shear strength vs. density plot, the existing data for composite lattice cores

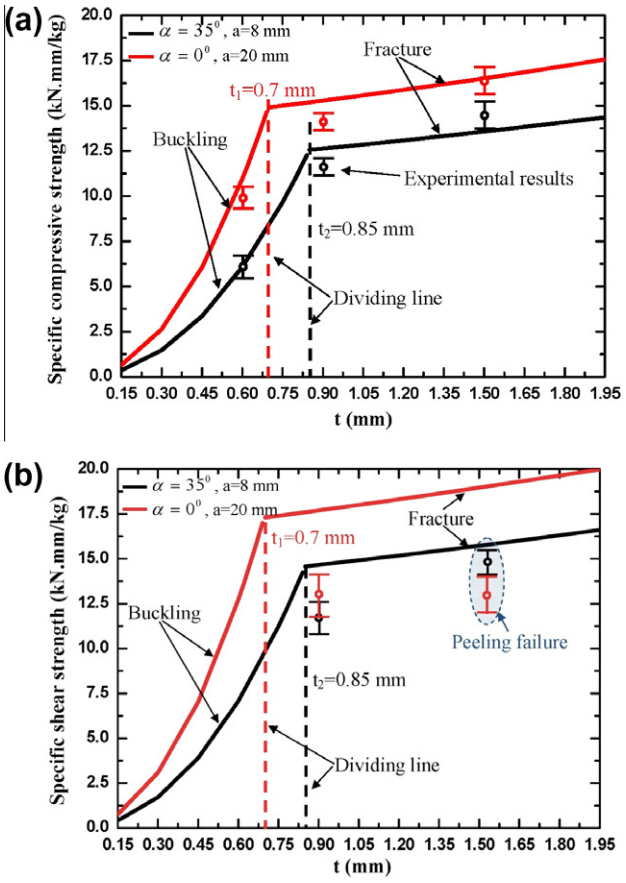


Fig. 11. The plots of (a) specific compressive strength, (b) specific shear strength as functions of struts thickness $t$, including buckling and fracture failure. Here, it was assumed that $b = 4.75$ mm, $d_e = 3.2$ mm, $h = 12$ mm, $l = 14$ mm, $\theta = 45°$. The analytical predictions are plotted as solid lines for lattice structures with different $\alpha$ and $a$. The oblique truss core (design 1) and vertical truss core are considered in the figure. Experimental data are also shown.

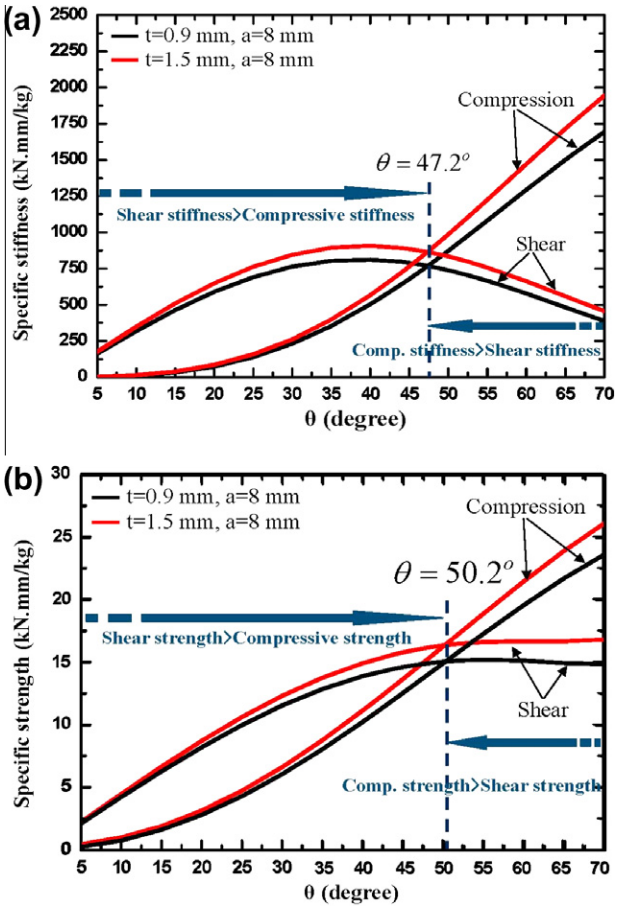


Fig. 12. The plots of (a) specific stiffness and (b) specific strength as functions of angle $\theta$ for lattice truss core. In this case, $b = 4.75$ mm, $d_e = 3.2$ mm, $h = 12$ mm, $l = 14$ mm, $\theta = 45°$ and $\alpha = 35°$.

other than the current work were grouped [12,13,20] and marked "Composite lattice truss core (past)". The data points are located mainly in the very low-density region of the chart. In the current study, the pyramidal truss-like core is heavier and stronger compared with the previously studied composite lattice truss cores. The large adhesion area created in the current manufacturing technique can transfer larger forces from the face sheets to the truss cores without damaging the face sheets or failing the bonds. Fig. 14 compares the shear strength of composite lattice structures reported in the literature. The results are presented in the form of shear strength vs. density, and different failure mechanisms are identified. Experimental results are also presented when available. As shown in Fig. 14, the composites lattice cores made using the LCB method provide no advantage over lattice cores fabricated using other techniques at low core relative densities. However, lattice cores with density >4.5% made using the LCB method have significantly improved shear strength compared with their counterpart lattice core made using other techniques. Thus, the present method provides a novel fabrication and prototyping method for carbon fiber composite lattice cores with high relative density, without comprising lattice core strength and performance.

## 8. Concluding remarks

A novel method for fabrication and prototyping of carbon fiber composite lattice cores using LBC was presented. Corrugated carbon fiber composite core is cut to form a near-pyramidal truss-like structure by high-energy laser. The bonding area is greater than previous pyramidal composite core structures. Out-of-plane compression and shear experiments were conducted to explore the mechanical properties and failure mechanisms, and analytical models were presented. In general, good agreement between the measurements and predictions was observed. Under crushing, Euler buckling, delamination and strut fracture were identified to govern the lattice structure strength. Delamination and fracturing of struts were observed under shear loading for the struts incorporating axial-direction fibers (namely, "oblique design 1" and "vertical"). No evidence

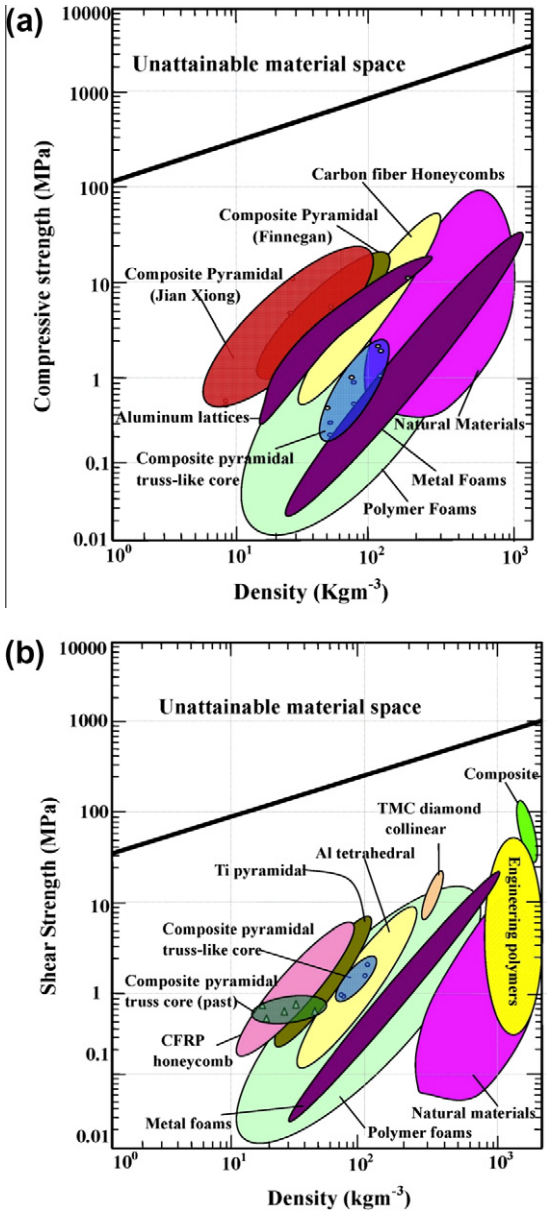


Fig. 13. An Ashby-style plot of (a) compressive strength and (b) shear strength as functions of density for a range of engineering materials. The data for the oblique and vertical pyramidal truss from this study are included along with comparable measurements for other competing cellular material.

of bond failure was observed during compression or shear loading.

It was demonstrated that laser cut cores can substantially increase the upper limit of shear strength for higher relative density pyramidal truss core. In the vertical case, it might be possible to improve the overall mechanical properties by placing more fibers parallel to the strut direction, since only half the fibers are currently so aligned. The present method can be used to fabricate carbon fiber composite panels with lattice cores for lightweight and multifunctional applications.

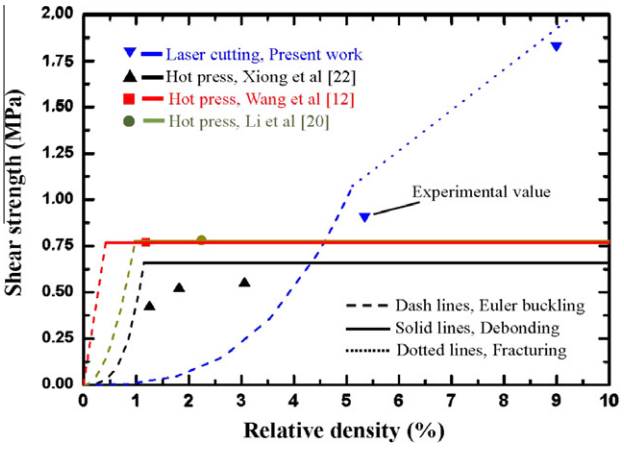


Fig. 14. Comparison of the shear strength for different carbon fiber composite pyramidal truss cores made by other method subjected to shear loading. Here, Euler buckling is shown by a dashed line, bonding failure by a solid line, and strut fracture by dotted lines. Wang et al. [12] and Li et al. [20] provided only one experimental result. In both cases, the shear strength was governed by bonding failure.

## Acknowledgements

The authors thank Dr. Jim Papadopoulos and Dr. Hamid Nayeb-Hashemi for fruitful discussions. The work was supported in part by the National Science Foundation of China under Grant Nos. 90816024, 10872059 and 11002041, the Major State Basic Research Development Program of China (973 Program) under Grant No. 2011CB610303, the Fundamental Research Funds for the Central Universities Grant No. HIT. NSRIF. 2010069, and the Excellent Teams Program at Harbin Institute of Technology. L.M. acknowledges the New Century Program for Excellent University Talents under Grant No. NCET-08-0152. A.V. acknowledges support by the US Air Force Office of Scientific Research under AFOSR YIP grant award, #FA 9550-10-1-0145 and technical direction of Dr. Joycelyn Harrison. J.X. also gratefully acknowledges the Young Scholar Prize awarded by MOE of China (AUDQ1010000611) and the China Scholarship Council (CSC).

## Appendix A. Derivation of compressive and shear stiffness and strength

### A.1. Compressive stiffness and strength

For an imposed displacement $\delta_z$ in the $z$ direction, $\delta_x = 0$, $\delta_y = 0$, $\delta_z \neq 0$. The axial force $F_A$ and shear force $F_S$ in a strut are given by elementary beam theory as

$$F_A = \frac{E_s dt \Delta l_{AB}}{l_{AB}} = \frac{E_s dt \sin\theta \cos^2\alpha}{l}\delta_z,$$

$$F_S = \frac{12E_s I \cos^3\alpha\sqrt{1-\sin^2\theta\cos^2\alpha}}{l^3}\delta_z \qquad \text{(A1)}$$

where $E_s$ denotes the apparent elastic modulus of individual struts and $I = dt^3/12$. Here it is assumed that the apparent length is $l \sin\theta$ under buckling. It should be noted that the apparent length for a thin composite struts depends on the end condition, and the fiber ply sequence is generally longer than the length assumed above and needs to be measured experimentally or using detailed finite element analysis. The total resisting force of the truss structure against compression $F_z$ can be obtained using the equilibrium of forces.

$$F_z = 4F_A[\sin\theta\cos\alpha + (F_S/F_A)\sqrt{1-\sin^2\theta\cos^2\alpha}] \tag{A2}$$

The nominal stress in the pyramidal truss-like core structure is $\sigma_z = F_z/A$, and the nominal strain of the structure is $\varepsilon_z = \delta_z/(h+t)$. The area of the unit cell is $A = WL$.

*A.1.1. Euler buckling of the struts*

The Euler buckling load of an end-clamped strut subjected to axial load can be estimated from

$$F_A = F_{zE} = \frac{\pi^2 E_s dt^3 \cos^2\alpha}{3l^2} \tag{A3}$$

*A.1.2. Fracture of the struts*

An upper limit for the failure load of the composite struts is $F_A = F_{zC} = \sigma_C dt$, where $\sigma_c$ is expected to vary substantially as a function of fiber angle for narrow composite struts [16], and was measured experimentally in our study.

*A.2. Shear stiffness and strength*

Applying a unit deflection $\delta_x$ in direction $x$ and constraining $\delta_y$ and $\delta_z$ to be zero, gives rise to a shear angle $\gamma_x$ and a resultant force $F_x$. These forces can be estimated using the classical beam theory as

$$F_A = \frac{E_s dt\cos^2\alpha\cos\theta}{l}\delta_x,$$
$$F_{St} = \frac{12E_s I_t\cos^3\alpha\sqrt{1-\cos^2\alpha\cos^2\theta}}{l^3}\delta_x,$$
$$F_{Sd} = \frac{12E_s I_d\cos^3\alpha}{l^3}\delta_x \tag{A4}$$

where $F_{St}$ and $F_{Sd}$ are force components under shear deformation, $I_t = dt^3/12$ and $I_d = td^3/12$. The total resisting force of the truss core under shear was obtained using the energy method.

$$F_x = 4F_A\left(\cos\theta\cos\alpha + \frac{F_{St}}{F_A}\sqrt{1-\cos^2\theta\cos^2\alpha} + \frac{F_{Sd}}{F_A}\right) \tag{A5}$$

The nominal shear stress in the pyramidal truss structure is $\tau_x = F_x/A$. The nominal shear strain of the structure is $\gamma_x = \delta_x/(h+t)$.

## References


[1] Rathbun HJ, Zok FW, Waltner SA, Mercer C, Evans AG, Queheillalt DT, et al. Acta Mater 2006;54:5509.
[2] Wei Z, Dharmasena KP, Wadley HNG, Evans AG. Int J Impact Eng A 2007;34:1602.
[3] Cote F, Deshpande VS, Fleck NA, Evans AG. Int J Solid Struct 2006;43:6220.
[4] Lee BK, Kang KJ. Scripta Mater 2009;60:391.
[5] Russell BP, Deshpande VS, Wadley HNG. J Mech Mater Struct 2008;3:1315.
[6] Moongkhamklang P, Deshpande VS, Wadley HNG. Acta Mater 2010;58:2822.
[7] Suralvo M, Bouwhuis B, Mccrea JL, Palumbo G, Hibbard GD. Scripta Mater 2008;58:247.
[8] Russell BP, Liu T, Fleck NA, Deshpande VS. J Appl Mech 2011;78. 031008-1.
[9] Jacobsen AJ, Carter WB, Nutt S. Acta Mater 2008;56:2540.
[10] Ajdari A, Haghpanah B, Papadopoulos J, Hashemi HN, Vaziri A. Int J Solids Struct 2012;49:1413.
[11] Schaedler TA, Jacobsen AJ, Torrents A, Sorensen AE, Lian J, Greer JR, et al. Science 2011;334:962.
[12] Wang B, Wu LZ, Ma L, Sun YG, Du SY. Mater Des 2010;31:2659.
[13] Xiong J, Ma L, Wu LZ, Wang B, Vaziri A. Compos Struct 2010;92:2695.
[14] Yin S, Wu LZ, Ma L, Nutt S. Compos Struct 2011;93:3104.
[15] Lee BC, Lee KW, Byun JH, Kang KJ. Composites Part B 2012;43:317.
[16] Finnegan K, Kooistra G, Wadley HNG, Deshpande VS. Int J Mater Res 2007;98:1264.
[17] Queheillalt DT, Murty Y, Wadley HNG. Scripta Mater 2008;58:76.
[18] Evans AG, Huchinson JW, Fleck NA, Ashby MF, Wandley HNG. Prog Mater Sci 2001;46:309.
[19] Ashby MF, Brechet YJM. Acta Mater 2003;51:5801.
[20] Li M, Wu LZ, Ma L, Wang B, Guan ZX. J Mater Sci Technol 2011;27:570.
[21] Xiong J, Ma L, Wu LZ, Liu JY, Vaziri A. Composites Part B 2011;42:938.
[22] Xiong J, Ma L, Pan SD, Wu LZ, Papadopoulos J, Vaziri A. Acta Mater 2012;60:1455.
[23] Wei Z, Deshpande VS, Evans AG, Dharmasena KP, Queheillalt DT, Wadley HNG, et al. J Mech Phys Solids 2008;56:2074.
[24] Feih S, Mathys Z, Gibson AG, Mouritz AP. Composites Part A 2007;38:2354.
[25] Velea MN, Wennhage P, Lache S. Mater Des 2012;36:679.
[26] Mohr D, Xue Z, Vaziri A. J Mech Mater Struct 2006;1:581.
[27] Xue Z, Vaziri A, Hutchinson JW. Comput Model Eng Sci 2005;10:79.
[28] Vaziri A, Xue Z. J Mech Mater Struct 2007;2:1743.
[29] Kazemahvazi S, Tanner D, Zenkert D. Compos Sci Technol 2009;69:920.
[30] Kazemahvazi S, Tanner D, Zenkert D. Compos Sci Technol 2009;69:913.
[31] Deshpande VS, Fleck NA. Int J Solids Struct 2001;38:6275.
[32] Wadley HNG, Fleck NA, Evans AG. Compos Sci Technol 2003;63:2331.
[33] ASTM: C365 Standard test method for flatwise compressive properties of sandwich cores. West Conshohocken (PA): ASTM International; 2006.
[34] ASTM: C273 Standard test method for shear properties of sandwich core materials. West Conshohocken (PA): ASTM International; 2006.